Solvothermal Synthesis of Metastable γ-MnS Hollow Spheres and Control of Their Phase

Shuijin Lei,[a,b] Kaibin Tang,*[a,b] Qing Yang,[a,b] and Huagui Zheng[b]

Keywords: Manganese / Nanostructures / Semiconductors / Solvothermal synthesis

A solvothermal route has been developed to prepare metastable wurtzite-structure γ-MnS hollow spheres from anhydrous manganese chloride, sulfur powder, and potassium borohydride in ethylene glycol at 150–180 °C. The metastable γ-MnS and stable α-MnS were characterized by X-ray diffraction, X-ray photoelectron spectroscopy, field-emission scanning electronic microscopy, scanning electron microscopy, transmission electron microscopy, and photoluminescence. Experiments show that the reaction temperature, the solvent, and the concentration and reducibility of the reductant are the crucial factors affecting the phase of the product. A possible growth mechanism for the hollow sphere is proposed.

Introduction

In recent years, inorganic and inorganic–organic hybrid hollow spheres of nanometer or submicrometer size have attracted considerable attention because of their potential applications in a broad range of areas, such as delivery vehicles for the controlled release of various substances, for example drugs, cosmetics, dyes, and inks, and for the protection of biologically active macromolecules, artificial cells, catalysts, fillers, coatings, pigments, light-weight structural or low density materials, and waste removal owing to their low density, large specific area, mechanical and thermal stability, and surface permeability.[1–5] A variety of chemical and physicochemical approaches have been employed to prepare hollow spheres, for example polymer, oxide, glass, and ceramic materials, including nozzle systems to dispense individual liquid droplets of uniform size (e.g. spray drying or pyrolysis),[6] emulsion/phase separation techniques (usually associated with sol-gel processing),[7] emulsion/interfacial polymerization strategies,[8] and self-assembly routes.[9]

Manganese sulfide (MnS), is a VIIB–VIA dilute magnetic semiconductor with a wide gap [bandgap energy: E_g (T = 0) ≈ 3.7 eV],[10] which has potential applications in solar cells, as a window/buffer material, and in short-wavelength optoelectronic materials. MnS usually has three polymorphs:[11] α-MnS, with a rock-salt structure, and the metastable phases β-MnS, with a zincblende structure, and γ-MnS, with a wurtzite structure. During equilibrium growth techniques, MnS crystallizes in the stable α phase. Both of the latter phases are antiferromagnetic, with Néel temperatures of 152 K (β-phase) and 90 K (γ-phase), and are transformed irreversibly into stable α-MnS upon heating.[12–16]

In previous studies, MnS is usually prepared by the direct reaction of manganese (Mn) and sulfide in an evacuated tube at high temperatures (above 800 °C).[17] β- and γ-MnS bulk phases have been prepared in polycrystalline form by low temperature chemical synthesis or evaporation.[18,19] The direct synthesis of polycrystalline β- and γ-MnS has also been reported by gas source molecular-beam epitaxy (MBE).[13,14] Metastable MnS thin films, which consist of nanocrystallite domains with mixed cubic and hexagonal phases, have been prepared by adopting a chemical bath deposition (CBD) method,[20,21] and recently a solvothermal route has been used to grow stable α-MnS and rod-like metabstable β- and γ-MnS nanocrystallites.[22] α-MnS nanocrystallites have also been prepared by a colloidal synthesis route by the reaction of $MnCl_2$ and $S[Si(CH_3)_3]_2$ in trioctylphosphane oxide,[23] and α-MnS nanorods have been prepared by a hydrothermal method from the elements (manganese and sulfur powder).[24] However, to the best of our knowledge, the metastable γ-MnS hollow sphere structure has not been reported.

In this paper, metastable γ-MnS hollow spheres are prepared by a developed solvothermal reaction at 150–180 °C from anhydrous manganese chloride ($MnCl_2$), sulfur powder, and potassium borohydride (KBH_4) as the reactants and ethylene glycol (EG) as the solvent. The phase of the as-formed MnS crystallites is influenced by the solvent, the reaction temperature, and the concentration and reducibility of the reductant.

[a] Nanomaterial and Nanochemistry, Hefei National Laboratory for Physical Sciences at Microscale, University of Science and Technology of China,
Hefei, Anhui 230026, P. R. China
Fax: +86-551-360-1791
E-mail: kbtang@ustc.edu.cn
[b] Department of Chemistry, University of Science and Technology of China,
Hefei, Anhui 230026, P. R. China

  DOI: 10.1002/ejic.200500442

Results and Discussion

Figure 1 shows the XRD patterns of as-prepared MnS powders. The samples shown in parts a–d of Figure 1 were prepared in EG. The diffraction peaks in Figure 1a can be indexed as the hexagonal γ-MnS with lattice constants a = 3.981 and c = 6.423 Å, which are close to those reported for γ-MnS [Joint Committee on Powder Diffraction Standards (JCPDS), Powder Diffraction File No. 40-1289: a = 3.979 and c = 6.446 Å]. The average crystallite size of γ-MnS is about 30 nm, as calculated from the Debye–Scherrer formula. Figure 1 (parts b–d) are the XRD patterns of the samples in which α-MnS and γ-MnS are coexistent. The peak marked by an asterisk in part c of Figure 1 is derived from $MnCO_3$. In Figure 1 (e), the XRD pattern of the product synthesized in $N_2H_4{\cdot}H_2O$, can be indexed as the cubic α-MnS (RS) with a = 5.216 Å (JCPDS, Powder Diffraction File No. 06-0518: a = 5.224 Å). We found that α-MnS gradually becomes the dominant phase with an increase of the reaction temperature, the concentration, and reducibility of the reductant, or the complexing ability of the solvent.

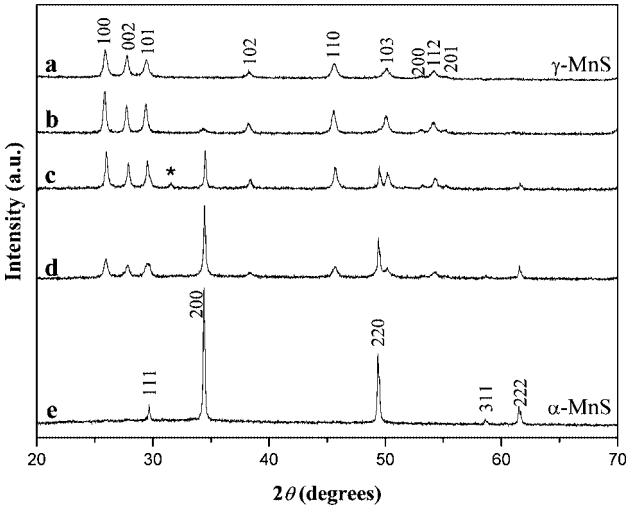

Figure 1. XRD patterns of the as-prepared MnS samples with different phase(s) synthesized: (a) in EG at 180 °C with a 3:5 molar ratio of S and KBH_4; (b) in EG at 240 °C with a 3:5 molar ratio of S and KBH_4; (c) in EG at 260 °C with a 3:10 molar ratio of S and KBH_4; (d) in EG at 260 °C with a 3:20 molar ratio of S and KBH_4; (e) in EA at 180 °C.

Figure 2 shows the XPS spectrum of as-synthesized γ-MnS. The binding energies of Mn $2p_{3/2}$ and S 2p were found to be 641.3 and 161.3 eV, respectively, which is consistent with the values reported in the literature.[25] There are also peaks for C reference and O impurity, due to the surface absorption of the samples exposed to air during processing of the samples. Direct elemental analysis for the composition of the sample was provided by ICP-AES, which gave an Mn/S molar ratio of 1:1.034. These results show that the product is stoichiometric.

Figure 3 (parts a and b) shows TEM images of the as-prepared γ-MnS, which reveal that the product consists of hollow spheres 300–500 nm in diameter; the wall thickness around the shell is about 50 nm. The strong contrast between the dark edges and pale centers is evidence of their hollow structures.[1d,2b,26,27] The direct observation of a broken sphere, as shown in Figure 3b, provides the most powerful proof of the hollow nature. The corresponding SAED pattern of the γ-MnS hollow sphere in Figure 3 (a) shows seven diffuse diffraction rings, which can be characterized as the (100), (002), (101), (102), (110), (103), and (112) planes from inner to outer (Figure 3, c) and further reveals the hexagonal γ-MnS polycrystals. The morphology of the sample synthesized in EG at 260 °C with a 3:10 molar ratio of S to KBH_4 was also examined. It consists of γ-MnS hollow spheres and α-MnS cubes. Figure 3 (d) presents the hollow and solid-sphere image of γ-MnS that was prepared using manganese chloride tetrahydrate ($MnCl_2{\cdot}4H_2O$) instead of anhydrous $MnCl_2$. The hollow spheres are clearly far fewer than the solid spheres. Figure 3 (e) gives the TEM image of α-MnS solid spheres prepared in EA at 180 °C. If the solvent is changed to EN, then α-MnS aggregates consisting of many micron-sized rods are obtained. Figure 3 (f) presents the TEM image of an individual rod aggregate. The corresponding ED pattern of a single rod (marked by an arrow) reveals that the as-prepared sample is well crystallized (see the inset).

Figure 4 shows the FE-SEM image of the γ-MnS broken hollow sphere. From this image, we can observe that the hollow sphere is structured with a lot of smaller particles, which are about 30–40 nm in size. Figure 4 (b) is the SEM image of γ-MnS hollow spheres and solid spheres. According to the difference of the hollow and solid sphere images, it can also be determined that the hollow spheres are in a very minor amount. The SEM photographs shown in Figures 4c and 4d are α-MnS solid sphere and α-MnS rod aggregates, respectively, which correspond to the samples of Figure 3 (parts e and f, respectively).

Figure 5 shows the room temperature PL spectra of the as-prepared γ-MnS hollow spheres (Figure 5, a) and α-MnS rod aggregates (Figure 5, b) with the same excitation wavelength of 365 nm (a filter with 500 nm wavelength was needed for γ-MnS). Figure 5 (a) exhibits a relatively strong and wide emission band peaking at about 720 nm (1.7 eV). In Figure 5 (b), an emission peaking at 435 nm (2.8 eV) can be observed, which is similar to the bandgap of the bulk counterpart.[23]

Table 1 summarizes the experiments and the effects of changing the solvent, the reaction temperature, and the concentration and reducibility of the reductant on the phase of the product.

From the results above, it can be seen that the optimum reaction temperature is 150–180 °C. When the reaction was performed in EG at 180 °C with a 3:5 molar ratio of S and KBH_4, γ-MnS hollow spheres were formed after five hours, whereas if the reaction temperature was reduced to 150 °C, then the reaction time had to be prolonged to 20 hours to produce pure γ-MnS. In this reaction system, KBH_4 is vital to prepare γ-MnS, and if the reaction temperature was increased above 200 °C, α-MnS appeared. In the range of 200–260 °C, the higher the temperature the greater the amount of α-MnS is present in the product. In this reaction

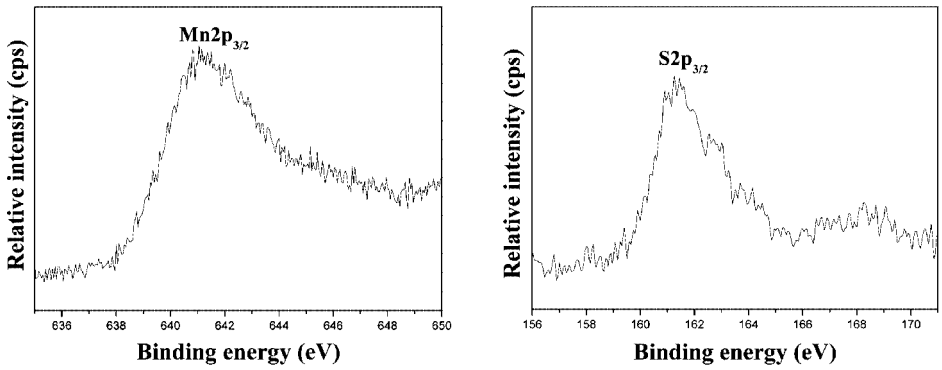

Figure 2. XPS spectra of the as-synthesized γ-MnS hollow spheres.

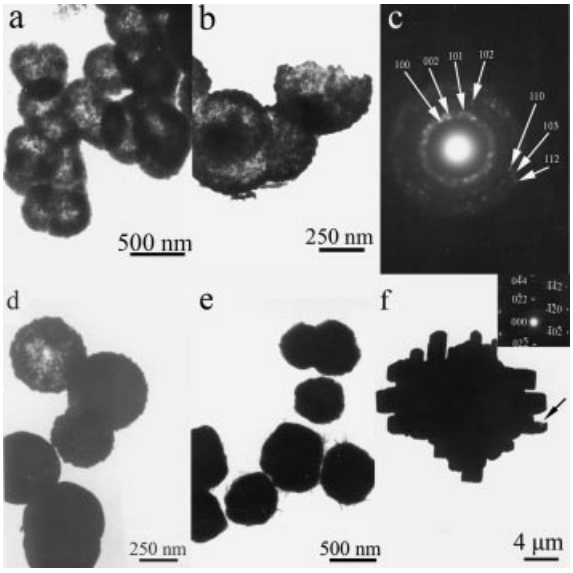

Figure 3. TEM images of as-prepared samples: (a) γ-MnS hollow spheres with anhydrous $MnCl_2$ as the reactant; (b) γ-MnS broken hollow sphere; (c) ED pattern for (a); (d) γ-MnS hollow spheres and solid spheres with $MnCl_2{\cdot}4H_2O$ as the reactant; (e) α-MnS spheres with EA as the solvent; (f) α-MnS rod aggregates with EN as the solvent (inset: the corresponding ED pattern of the single rod marked by an arrow).

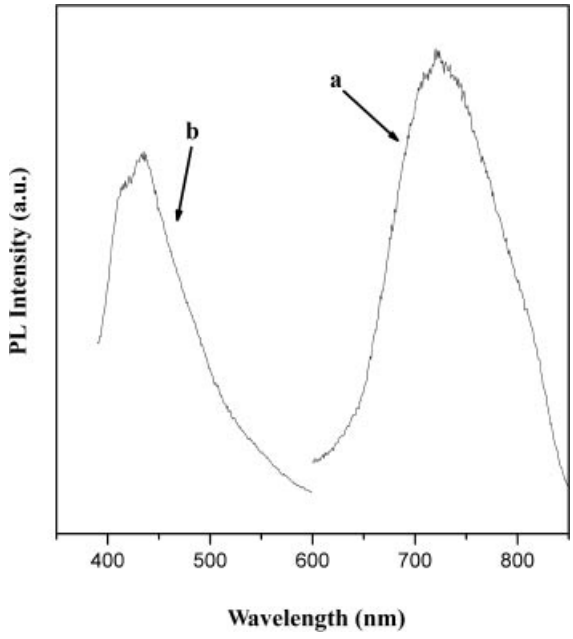

Figure 5. PL spectrum (λ_{ex} = 365 nm) of the as-synthesized samples for: (a) γ-MnS hollow spheres, and (b) α-MnS rod aggregates with EN as the solvent.

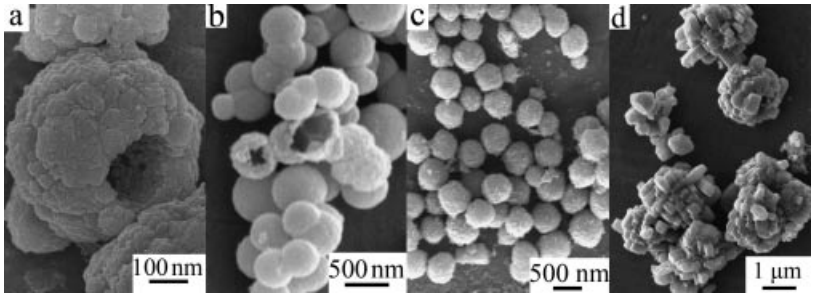

Figure 4. (a) FE-SEM image of γ-MnS broken hollow sphere and SEM images; (b) γ-MnS hollow spheres and solid spheres when $MnCl_2{\cdot}4H_2O$ was used as the reactant; (c) α-MnS solid spheres when EA was used as the solvent; (d) α-MnS rod aggregates when EN was used as the solvent.

system, the γ phase is readily obtained at low temperature and the α phase at high temperature as at higher reaction temperatures the metastable γ-MnS is transformed into stable α-MnS.

When the system was maintained at an appropriate reaction temperature above 200 °C, and the amount of KBH_4 was increased gradually, we also found that the content of α-MnS in the product increased. It must be pointed out

Table 1. Effects of the solvent, the reaction temperature, and the concentration and reducibility of the reductant on the phase of product.

Reaction temperature [°C]	Solvent[a]	Molar ratio of $MnCl_2/KBH_4$ or the amount of $N_2H_4{\cdot}H_2O$	Reaction time [h]	Product[b]
150	EG	3:5	>20	γ-MnS
180	EG	3:5	>5	γ-MnS
220–240	EG	3:5	12	γ-MnS*, α-MnS
250–260	EG	3:10~15	12	γ-MnS, α-MnS
250–260	EG	3:20	12	γ-MnS, α-MnS*
180	EG	5 mL of $N_2H_4{\cdot}H_2O$	12	γ-MnS, α-MnS*
180	EG	10 mL of $N_2H_4{\cdot}H_2O$	12	α-MnS
180	EA	3:5	12	α-MnS
180	EN	3:5	12	α-MnS

[a] EG stands for ethylene glycol, EA for ethanol amine, and EN for ethylenediamine. [b] * indicates the dominant phase in the product.

that a large excess of KBH_4 (e.g. 10–20 mol) and a high reaction temperature (e.g. 240–260 °C) also resulted in the appearance of $MnCO_3$. If KBH_4 was replaced by the stronger reductant $N_2H_4{\cdot}H_2O$, α-MnS was obtained easily along with a small quantity of γ-MnS; an increase of the amount of $N_2H_4{\cdot}H_2O$ gave pure α-MnS. These results reveal that a stronger reductant and higher concentration are beneficial for the formation of α-MnS.

The influence of the solvent on the phase of the product was also studied. If EA and EN were used as the solvent, keeping the other conditions identical, the sample obtained was α-MnS. The amido groups in EA and EN, which have a strong N-chelation ability, form a relatively stable Mn^{2+} complex, which is favorable for the transformation to the stable form. $N_2H_4{\cdot}H_2O$ also has an amido group, so when it was used as the reductant α-MnS also formed.

Scheme 1 illustrates the possible mechanism for the formation of γ-MnS hollow spheres. In the detailed procedure, solid-state sulfur powder could be transformed into tiny spherical sulfur liquid droplets dispersed in the EG solvent to form a heterogeneous liquid–liquid two-phase mixture on account of the surface tension[28,29] at temperatures above the melting point of sulfur (120 °C at normal atmosphere) in the autoclave. Sulfur acts as the template for the fabrication of γ-MnS hollow spheres, as well as the sulfur source. Around the sulfur liquid droplets, BH_4^- and Mn^{2+} dissolved in EG react with them on the surface. BH_4^- can readily serve as a hydride and electron transfer agent,[30] which reduces elemental S to S^{2-} and forms MnS with Mn^{2+}. Experiments showed that elemental S can be reduced to S^{2-} by BH_4^- even in the absence of Mn^{2+} ions in this system, although Mn^{2+} ions could shift the redox reaction equilibrium to the forward reaction direction. The interface reaction results in the consumption of liquid sulfur droplets and the formation of γ-MnS hollow spheres. With the increase of the reaction temperature and the amount of KBH_4, α-MnS cubes were simultaneously obtained besides γ-MnS hollow spheres. The anisotropy of hexagonal γ-MnS should support the aggregation of the γ-MnS nanoparticles into spheres, while the formation of α-MnS cubes is maybe due to the growth character based on the cubic structure of α-MnS. In addition, compared with γ-MnS, α-MnS is high-temperature phase, and its nucleation velocity is smaller, so it is relatively difficult to be aggregated and tends to form bigger crystals.

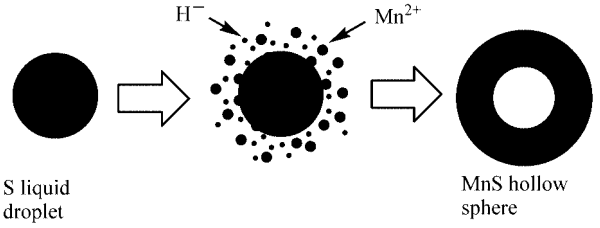

Scheme 1. Schematic illustration of the possible growth mechanism for γ-MnS hollow spheres.

The crystallization water of the reactant evidently affects the morphology of the final product. When $MnCl_2{\cdot}4H_2O$ was used without prior dehydration, then γ-MnS solid spheres and a small number of hollow spheres were obtained, as shown in Figure 3 (c) and Figure 5 (a). In the presence of the crystallization water, the reaction was accelerated owing to hydrolysis of BH_4^- with the generation of hydrogen. This reaction even occurs very rapidly at room temperature. What's more, the higher the water temperature and the smaller the ratio of water to borohydride, the more rapid the hydrolysis.[31–34] In this system most of the sulfur probably reacts with BH_4^- and Mn^{2+} before the formation of the tiny liquid sulfur droplets.

$$4S_{(s)} + BH_4^- + 2H_2O \rightarrow BO_2^- + 4S^{2-} + 8H^+$$

$$S^{2-} + Mn^{2+} \rightarrow MnS$$

This causes the fabrication of the γ-MnS solid spheres. With an increase of temperature, the remaining sulfur forms the liquid droplets that act as the template for the formation of γ-MnS hollow spheres.

Sulfur is readily soluble in EA or EN therefore the liquid sulfur droplets can't form and hence the γ-MnS hollow spheres aren't obtained.

Conclusions

In summary, metastable γ-MnS submicrometer hollow spheres and α-MnS spheres have been successfully synthesized by a solvothermal method. The reaction temperature, the solvent, and the concentration and reducibility of the reductant strongly influence the phase(s) of the product. The photoluminescence of the γ-MnS hollow spheres and α-MnS rod aggregates has been investigated at room temperature using the same excitation line at 365 nm. A possible growth mechanism for the hollow structure has also

been tentatively proposed on the basis of the experimental results. A further exploration of the growth mechanism for the hollow structure, the control of the reaction kinetics, and the morphology of α-MnS are underway.

Experimental Section

All the chemical reagents were of analytical grade and were purchased from Shanghai Chemical Reagent Company and used without further purification. Anhydrous $MnCl_2$ was obtained by the dehydration of $MnCl_2·4H_2O$ with thionyl chloride as dehydrating agent.

Preparation of Metastable γ-MnS Hollow Spheres: Typically, a slight excess of anhydrous $MnCl_2$ (0.4 g) was dissolved in 20 mL of EG. Sulfur powder (0.096 g) and KBH_4 (0.27 g) with a 3:5 molar ratio, together with the above solution, were put into a 60-mL Teflon-lined autoclave, which was then filled with EG up to 85% of the total volume. The autoclave was sealed quickly and maintained at 150–180 °C for 5–24 h, and then cooled to room temperature naturally. The products were filtered off, washed with absolute ethanol and distilled water several times to remove impurities, and dried in vacuo at 60 °C for 4 h.

When 10 mL of 80% (wt.) hydrazine hydrate ($N_2H_4·H_2O$) solution was used instead of KBH_4, or the solvent EG was replaced by ethanol amine (EA) or ethylenediamine (EN), then α-MnS was obtained.

Sample Characterization: The X-ray powder diffraction (XRD) patterns were recorded on a Philips X'pert PRO SUPER diffractometer with Cu-K_α radiation (λ = 1.541874 Å). The X-ray photoelectron spectra (XPS) were recorded on a VGESCALAB MK II X-ray photoelectron spectrometer, using Mg-K_α radiation as the excitation source. Field-emission scanning electronic microscopy (FE-SEM) measurements were recorded with a field-emission microscope (JEOL, 7500B) operating at an acceleration voltage of 10 kV. The scanning electron microscopy (SEM) images were taken with an X-650 scanning electronic microanalyzer. The transmission electron microscopy (TEM) images and selected area electron diffraction (SAED) patterns were obtained with a Hitachi H-800 transmission electron microscope, using an accelerating voltage of 200 kV. Photoluminescence (PL) spectra of the sample were obtained on a Hitachi F-4500 fluorescence spectrophotometer at room temperature.

Acknowledgments

Financial support by the National Natural Science Foundation of China, the 973 Projects of China, and the Program for New Century Excellent Talents in Universities (NCET) is gratefully acknowledged.

[1] a) D. L. Wilcox, M. Berg, T. Bernat, D. Kellerman, J. K. Cochran, *Hollow and Solid Spheres and Microspheres: Science and Technology Associated with Their Fabrication and Application*, Materials Research Society Proceedings, MRS, Pittsburgh, PA, **1995**, p372; b) J. K. Cochran, *Curr. Opin. Solid State Mater. Sci.* **1998**, *3*, 474; c) H. Huang, E. E. Remsen, *J. Am. Chem. Soc.* **1999**, *121*, 3805; d) C. E. Fowler, D. Khushalani, S. Mann, *J. Mater. Chem.* **2001**, *11*, 1968.
[2] a) F. Caruso, *Chem. Eur. J.* **2000**, *6*, 413; b) F. Caruso, R. A. Caruso, H. Möhwald, *Science* **1998**, *282*, 1111.
[3] Z. Zhong, Y. Yin, B. Gates, Y. Xia, *Adv. Mater.* **2000**, *12*, 206.
[4] A. B. Bourlinos, M. A. Karakassides, D. Petridis, *Chem. Commun.* **2001**, *16*, 1518.
[5] K. H. Rhodes, S. A. Davis, F. Caruso, B. Zhang, S. Mann, *Chem. Mater.* **2000**, *12*, 2832.
[6] a) P. Tartaj, T. González-Carreño, C. J. Serna, *Adv. Mater.* **2001**, *13*, 1620; b) M. R. Al-Ubaidi, J. Anno, *Fusion Technol.* **1989**, *16*, 464; c) P. J. Bruinsma, A. Y. Kim, J. Liu, S. Baskarn, *Chem. Mater.* **1997**, *9*, 2507; d) Y. Lu, H. Fan, A. Stump, T. L. Ward, T. Rieker, C. J. Brinker, *Nature* **1999**, *398*, 223; e) M. Iida, T. Sasaki, M. Watanabe, *Chem. Mater.* **1998**, *10*, 3780.
[7] a) S. Schacht, Q. Huo, I. G. Voigt-Martin, G. D. Stucky, F. Schüth, *Science* **1996**, *273*, 768; b) K. J. Pekarek, J. S. Jacob, E. Mathiowitz, *Nature* **1994**, *367*, 258; c) J. G. Liu, D. L. Wilcox, *J. Mater. Res.* **1995**, *10*, 84.
[8] a) J. Hotz, W. Meier, *Langmuir* **1998**, *14*, 1031; b) K. B. Thurmond, T. Kowalewski, K. L. Wooley, *J. Am. Chem. Soc.* **1997**, *119*, 6656; c) M. Okubo, Y. Konishi, H. Minami, *Colloid Polym. Sci.* **1998**, *276*, 638.
[9] a) B. M. Discher, Y.-Y. Won, D. S. Ege, J. C.-M. Lee, F. S. Bates, D. E. Discher, D. A. Hammer, *Science* **1999**, *284*, 1143; b) M. Zhao, L. Sun, R. M. Crooks, *J. Am. Chem. Soc.* **1998**, *120*, 4877; c) M. S. Wendland, S. C. Zimmerman, *J. Am. Chem. Soc.* **1999**, *121*, 1389; d) K. B. Thurmond, *Biointerfaces* **1999**, *16*, 45; e) S. A. Jenekhe, X. L. Chen, *Science* **1998**, *279*, 1903.
[10] O. Goede, W. Heimbrodt, *Phys. Status Solidi B* **1988**, *146*, 11.
[11] C. Sombuthawee, S. B. Bonsall, F. A. Hummel, *J. Solid State Chem.* **1978**, *25*, 391.
[12] O. Goede, W. Heimbrodt, V. Weinhold, *Phys. Status Solidi B* **1987**, *143*, 511.
[13] M. Okajima, T. Tohda, *J. Cryst. Growth* **1992**, *117*, 810.
[14] B. J. Skromme, Y. Zhang, D. J. Smith, *Appl. Phys. Lett.* **1995**, *67*, 2690.
[15] L. Wang, S. Sivananthan, R. Sporken, *Phys. Rev. B* **1996**, *54*, 2718.
[16] S. W. Kennedy, K. Harris, E. Summerville, *J. Solid State Chem.* **1980**, *31*, 355.
[17] H. Wiedemeier, A. G. Sigal, *J. Cryst. Growth* **1969**, *6*, 67.
[18] O. Goede, W. Heimbrodt, V. Weinhold, *Phys. Status Solidi B* **1986**, *136*, K49.
[19] W. Heimbrodt, *Phys. Status Solidi B* **1989**, *154*, 405.
[20] M. A. Akhter, *Thin Solid Films* **1988**, *158*, 83.
[21] C. D. Lokhande, A. Ennaoui, P. S. Patil, *Thin Solid Films* **1998**, *330*, 70.
[22] J. Lu, P. F. Qi, Y. Y. Peng, Z. Y. Meng, Z. P. Yang, W. C. Yu, Y. T. Qian, *Chem. Mater.* **2001**, *13*, 2169.
[23] S. H. Kan, I. Felner, U. Banin, *Isr. J. Chem.* **2001**, *41*, 55.
[24] C. H. An, K. B. Tang, X. M. Lin, F. Q. Li, G. E. Zhou, Y. T. Qian, *J. Cryst. Growth* **2003**, *252*, 575.
[25] G. E Muilenberg, C. D. Wagner, W. M. Riggs, L. E. Davis, J. F. Moulder, *Handbook of X-ray Photoelectron Spectroscopy*, Physical Electronics Division, Perkin–Elmer Corp., New York, **1979**, p. 74.
[26] P. V. Braun, S. I. Stupp, *Mater. Res. Bull.* **1999**, *34*, 463.
[27] S. Dieluweit, D. Pum, U. B. Sleytr, *Supramol. Sci.* **1998**, *5*, 15.
[28] G. M. Barrow, *Physical Chemistry*, McGraw-Hill, New York, **1979**, ch. 21.
[29] R. B. Heslop, P. L. Robinson, *Inorganic Chemistry*, Elsevier, Amsterdam, **1963**, ch. 22.
[30] F. A. Cotton, G. Wilkinson, *Advanced Inorganic Chemistry*, 5th ed., Jonh Wiley & Sons, New York, **1988**, pp. 190–192.
[31] H. I. Schlesinger, H. C. Brown, A. E. Finholt, J. R. Gilbreath, H. R. Hoekstra, E. K. Hyde, *J. Am. Chem. Soc.* **1953**, *75*, 215.
[32] G. N. Glavee, K. J. Klabunde, C. M. Sorensen, G. C. Hadjipanayis, *Inorg. Chem.* **1995**, *34*, 28.
[33] G. N. Glavee, K. J. Klabunde, C. M. Sorensen, G. C. Hadjipanayis, *Langmuir* **1993**, *9*, 162.
[34] G. N. Glavee, K. J. Klabunde, C. M. Sorensen, G. C. Hadjipanayis, *Langmuir* **1994**, *10*, 4726.

Received: May 16, 2005
Published Online: September 5, 2005

